Mathematical Biosciences and Engineering

MBE, 19 (11): 11657–11674.
DOI: 10.3934/mbe.2022542
Received: 29 June 2022
Revised: 31 July 2022
Accepted: 04 August 2022
Published: 15August 2022

http://www.aimspress.com/journal/MBE

Research article

Computational analysis of cutting parameters based on gradient Voronoi model of cancellous bone

Wei Lin and Fengshuang Yang*

School of Mechanical and Vehicle Engineering, Changchun University, Changchun 130012, China

* **Correspondence:** Email: yangfs@ccu.edu.cn, linw@ccu.edu.cn; Tel: +8613756312716.

Abstract: Bone cutting is a complicated surgical operation. It is very important to establish a kind of gradient porous bone model in vitro which is close to human bone for the research of bone cutting. Due to the existing bone cutting researches are based on solid bone model, which is quite different from human bone tissue structure. Therefore, Voronoi method was used to establish a gradient porous bone model similar to real bone tissue to simulate the process of bone drilling in this paper. High temperature and large cutting force during bone drilling can cause serious damage to bone tissue. Urgent research on bone drilling parameters is necessary to reduce cutting temperature and cutting force. The finite element analysis (FEA) of Voronoi bone models with different gradients is carried out, and a Voronoi model which is similar to real bone tissue is obtained and verified by combining the cutting experiment of pig bone. Then orthogonal experiments are designed to optimize the cutting parameters of Voronoi bone model. The range method is used to analyze the influence weights of cutting speed, feed speed and tip angle on cutting temperature and cutting force, and the least square method was used to predict the cutting temperature and cutting force, respectively. The gradient porous bone model constructed by Voronoi method was studied in detail in this paper. This study can provide theoretical guidance for clinical bone drilling surgery, and the prediction model of bone drilling has practical significance.

Keywords: bone cutting; Voronoi method; cutting parameters; cutting temperature; cutting force; orthogonal experiments; range method; the least square method

1. Introduction

Bone cutting is a common surgical method in bone surgery. In the process of bone cutting, the temperature generated by the cutting directly affects the biological activity of bone material and the degree of thermal damage to the surrounding soft tissue, especially when the temperature of the bone in direct contact with the cutter reaches 47℃ and remains for more than 1min, thermal necrosis will occur immediately due to high temperature [1]. Thermal necrosis of bone materials and surrounding soft tissues can prolong and delay the patient's postoperative recovery time [2]. In addition, excessive stress also leads to the damage of bone tissue, cartilage tissue and muscle in the surrounding area of cutting, resulting in secondary damage [3,4]. Therefore, reducing the temperature and stress in the process of bone cutting is the urgent research. Bone is a kind of anisotropic material with low thermal conductivity, 0.16~12.8 $WM^{-1}\cdot K^{-1}$ [5,6]. These characteristics prevent heat dissipation during bone cutting, leading to the increase of bone temperature. Besides, the drilling mechanism is produced by a complex combination of cutting and extrusion at the drill point, and the cutting force, torque, and temperature must be kept below the critical level of osteonecrosis [7]. During bone drilling, there is the energy conversion, i.e., mechanical work (friction and shear deformation of bone) from cutters is converted into heat energy [1,8,9]. The cutting temperature and the cutting force generated depend on various cutting parameters, such as bit diameter, bit speed, and axial drilling force [10]. Davidson et al. investigated the effects of spindle speed, feed rate, screw angle, bit apex angle, and bit diameter on drilling temperature [11]. The results showed that spindle speed, feed rate and bit diameter had great influence on bone thermal properties, while screw angle and bit apex angle had relatively weaker influence on bone thermal properties. Chen et al. studied the influence of drilling parameters (feed rate and rotational speed) on bone temperature, and analyzed bone temperature distribution through experiments and numerical simulation of drilling process [12]. They pointed out that when the drilling speed was constant, the maximum temperature of bone decreased with the increase of feed rate, while when the feed rate was constant, the maximum drilling temperature increased with the increase of rotational speed, and the maximum temperature occurred in the cancellous bone near the cortical bone in their study. Karaca et al. found that the drilling temperature increased gradually in the process of increasing the drilling speed from 200 r/min to 1180 r/min when drilling the calf tibia [13]. However, the effects of cutting parameters on temperature were inconsistent. For example, some studies believed that when drilling speed was low, the temperature increased with the increase of drilling speed, while others believed that the temperature decreased with the increase of drilling speed [10].

The research showed that the cutting parameters also had great influence on the cutting force. Udiliak et al. evaluated the influence of bit tip angle and spindle speed on drilling force [14], and they concluded that bit tip angle was related to drilling force, while spindle speed had no obvious influence on it. At the same time, the feed speed was proportional to the drilling force. Alam et al. explored the influence of cutting depth, cutting speed and other parameters on cutting force in planar cutting of cortical bone based on FEA [15]. The results showed that lower cutting depth and sharp cutting tools can reduce cutting force. With the improvement of machining technology, the ultrasonic vibration method can effectively reduce the cutting temperature and cutting force. Wang et al. found that compared with conventional drilling methods, low-frequency vibration assisted drilling (frequency 5–20 Hz) had fewer and shorter microcracks, and the cutting heat was significantly reduced [16,17]. Zakrasas et al. conducted drilling experiments using pig ribs as samples, and the

results showed that the maximum temperature generated at vibration frequencies of 60–120 Hz was 14% lower than that generated by conventional cutting [18]. Ostaševičius et al. also conducted 10 drilling experiments (frequency 60–140 Hz), and the results showed that the drilling temperature was reduced by 21℃ when the frequency was 80 Hz [19]. Gupta et al. proved through ultrasound-assisted pig bone drilling experiment that the rotational speed of the bit had the greatest influence on the temperature rise, accounting for 46% of the total proportion [20]. Paktinat and Amini [21], Nosouni [22] et al. compared the drilling effect of vibration-assisted drilling with that of ordinary drilling, and conducted simulation and experimental research on drilling force. The results showed that in the test range, the vibration-assisted drilling effect was better. The axial force produced by ultrasonic assisted drilling was obviously lower than that produced by ordinary drilling. Optimizing the structure of bone cutting tools is also an effective method to reduce cutting heat and bone stress [23]. For example, micro-texture tools can effectively improve the situation of excessive cutting heat and cutting force in the process of bone cutting [24–26].

Human bone is composed of four layers of tissue, including periosteum, cortical bone (dense bone), cancellous bone (spongy or trabecular bone) and bone marrow [27,28]. In particular, cancellous bone is formed by porous structure similar to honeycomb and has a gradient distribution [29,30]. Cancellous bones have large interstitial spaces with porosity ranging from 50 to 90% [31]. Although cortical bone structure is nearly solid, it still has about 3–5% porosity [29]. In the existing literature, the bone model mostly adopts the solid model for finite element analysis. However, the continuum model is not fit for porous model such as bone. Because the Cauchy continuum model is the simplest mechanical model to describe the behavior of bone from a macroscopic point of view [32,33]. Indeed, the porous space inside bone tissue is filled with fluids, such as bone marrow, interstitial fluid, blood, etc., so bone tissue is a model of liquid-solid two-phase coexistence [33,34]. To be precise, bone tissue is considered to be an anisotropic material rather than an isotropic Cauchy continuum model. To correctly describe the behavior of bone tissue at the level of hundreds of micrometers, the geometric arrangement and porosity of bone interior are needed [33]. Therefore, it is inevitable to consider the effect of porous structure on cutting heat and force when conducting bone cutting research. The accuracy of the bone cutting model determines the described phenomena. But few studies have been reported on this topic. Therefore, a gradient porous structure of bone cutting model was constructed using Voronoi method in this paper, and the main research contents were as follows: 1) a gradient porous structure of bone cutting model was established based on Voronoi method, and the cutting temperature and cutting force were verified by FEA and cutting experiment; 2) orthogonal cutting experiments were designed to analyze the influence of cutting parameters on the Voronoi bone model; 3) The least square method is used to establish the prediction model of bone cutting temperature and cutting force.

2. Materials and methods

2.1. Construct the gradient porous bone model based on Voronoi method

Voronoi diagram, also called Tyson polygon or Dirichlet diagram, is a space segmentation method based on seed points. Given a finite set of points in the Euler plane $\{..., P_i, ... P_n\}$ [35,36], for each point P_i, the corresponding Voronoi unit contains all points in the Euler plane whose distance to P_i is less than or equal to any other point, and these points divide the Euler space into two parts. The

Voronoi diagram is determined by the number and distribution of seed points, the control of which is critical to the successful modeling of irregular porous scaffolds for a set of points in m-dimensional Euclidean space:

$$P = \{p_1, \ldots, p_n\} \in R^m,\ 2 \le n < \infty,\ p_i \neq p_j,\ i, j \in I_n = \{1, \ldots, n\} \tag{1}$$

Given that Voronoi diagram can be generated at any point in space and irregular structures can be established, Wang's team successfully obtained gradient porous structures based on the top-down design method of Voronoi Mosaic [37]. Han et al. also designed porous bone structure with gradient by using Voronoi method [38]. Based on these studies, a three-dimensional model of porous bone cutting with gradient is established by using Voronoi method in this paper. Therefore, python language was used to program three-dimensional Voronoi structure, and Python script was run in finite element software Abaqus2020 to construct porous bone tissue models with different gradients, as shown in Figure 1. The gradient bone model refers to the center of each structure as the benchmark. The closer to the center, the sparser the Voronoi units are, inversely, the closer to the edge of the strucutre, the denser the Voronoi units are. In this study, three gradients were set as 0.7, 0.8 and 0.9, respectively. The smaller the number is, the more obvious the gradient is. These designed gradient structures were used for bone cutting simulation analysis to select replacement models that were similar to real bone issue.

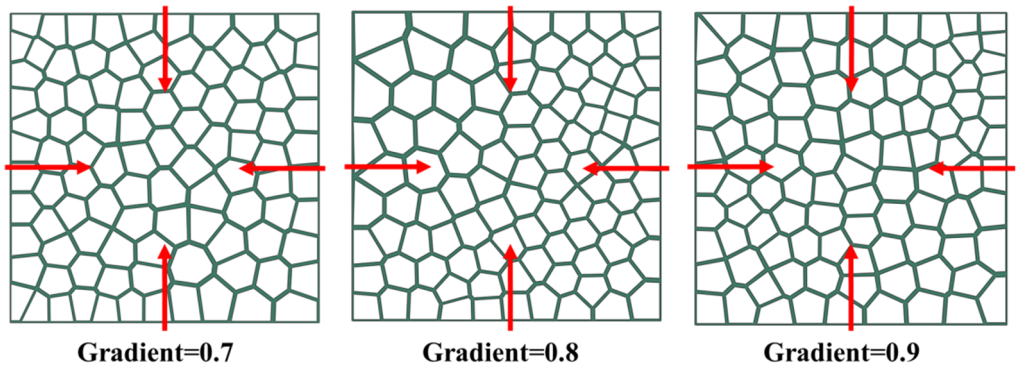

Figure 1. The gradient bone model based on Voronoi method.

2.2. FEA of gradient Voronoi bone

FEA has been widely used in bone tissue cutting. In the FEA, it is often necessary to define the thermodynamic properties of the model materials, and accurate material parameters can more truly simulate the cutting process. In this paper, it is assumed that the bone material was isotropic and had elastic-viscoplastic behavior for the prediction of cutting force and temperature. The drilling bit was assumed to be a clinically similar stainless steel material. Table 1 lists the thermodynamic performance parameters of the bone model and the drilling bit [12]. To describe the mechanical behavior of bone tissue, the Johnson-Cook (J-C) constitutive model was used, which took nonlinear strain hardening and strain rate sensitivity into account [39]. J-C model can be used to describe bone as an elastoplastic material with bilinear strain hardening [15], as shown in Eq (2). J-C model

parameters of bone materials are listed in Table 2 [15,16]:

$$\bar{\sigma} = (A + B\,\varepsilon^{n})\left(1 + C\,ln\frac{\dot{\varepsilon}}{\dot{\varepsilon}_0}\right)\left[1 - \left(\frac{T - T_r}{T_m - T_r}\right)^{m}\right] \tag{2}$$

In which $\bar{\sigma}$ is the material flow stress, ε is the equivalent plastic strain, T_m is the melting temperature of the material, T is the material temperature, T_r is the reference temperature, $\dot{\varepsilon}$ is the plastic strain rate, $\dot{\varepsilon}_0$ is the effective plastic strain rate of the quasi-static test and A, B, C, m, n are the material constants.

Generally, bone cutting heat comes from three regions: shear deformation zone, friction zone I and friction zone II, as shown in Figure 2(a). Shear deformation is caused by plastic deformation of bone. However, both friction zones are generated by contact between the drilling bit and the bone, and friction between the bone chips and the front slope creates zone I. Lateral friction with bone surface produces zone II. The shear deformation zone and friction zone I convert mechanical work to heat energy, but the energy of friction zone II is negligible if a sharp bit is used [1,9].

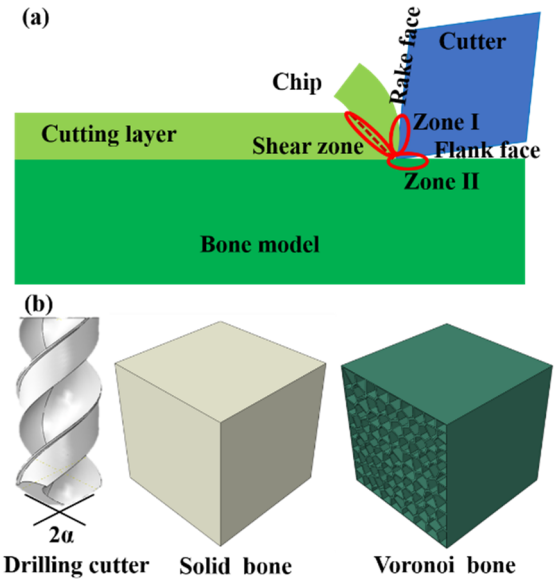

Figure 2. Bone cutting model: (a) Two-dimensional cutting heat model; (b) Three-dimensional models including drilling cutter, solid bone and Voronoi bone.

In the process of bone cutting, chip will be formed when the cutting edge contact with the bone surface. Consequently, it is necessary to set the failure criterion of bone material. In the simulation of bone drilling, shear damage failure criterion is usually selected. In this part, J-C damage model was used to separate the formation of wool chips, as shown in Eq (3). In the J-C damage model, damage occurs when parameter D exceeds 1 [22]. Table 3 shows parameters of the J-C damage model:

$$D = \sum \frac{\Delta\bar{\varepsilon}^{pl}}{\bar{\varepsilon}_f^{pl}} \tag{3}$$

In which $\Delta\bar{\varepsilon}^{pl}$ is the plastic tension increase and $\Delta\bar{\varepsilon}_f^{pl}$ is the tension needed for damage and is

calculated from Eq (4):

$$\bar{\varepsilon}_f^{pl} = \left(d_1 + d_2 \exp d_3 \frac{p}{q}\right)[1 + d_4 \ln\frac{\varepsilon_{pl}}{\dot{\varepsilon}_0}](1 + d_5 \frac{T - T_r}{T_m - T_r}) \tag{4}$$

In which p is the compressive stress, q is the von-misses stress, d_1 is initial failure strain, d_2 is exponential factor, d_3 is triaxiality factor, d_4 is strain rate factor, d_5 is temperature factor.

Table 1. Thermodynamic parameters of cancellous bone model and cutter [12].

elastic and thermal properties	cancellous bone	cutter
young modulus (MPa)	759	193000
Poisson's ratio	0.30	0.25
density (kg/m^3)	640	7990
thermal conductivity (W/m·K)	0.087	16.2
specific heat (J/kg·K)	1477	500
yield stress (MPa)	31.0	290
ultimate stress (MPa)	31.1	579
ultimate strain	0.07	0.003

Table 2. Parameters of cancellous bone Johnson-Cook model [15,16].

A	B	n	C	m	ε	T_r	T_m
50 MPa	101 MPa	0.72	0.059	1.56	0.001	945 K	293 K

Table 3. Johnson-Cook damage material constants.

d_1	d_2	d_3	d_4	d_5
-0.068	0.451	-0.952	0.036	0.697

2.3. Orthogonal cutting experiment scheme and FEA

This research focuses on analyzing the effects of cutting rotational speed V_c (Hereinafter referred to as cutting speed), feed speed V_f and tip angle α on bone cutting temperature and cutting force. Therefore, the orthogonal experiment scheme of establishing three-factor three-level numerical simulation is shown in Table 4.

Table 4. Orthogonal experimental scheme.

cutting parameters	Level 1	Level 2	Level 3
cutting speed V_c (mm/s)	10	15	20
feed speed V_f (mm/s)	0.5	1.0	1.5
tip angle 2α (°)	105	115	125

FEA was carried out using Abaqus2020 explicit dynamics, and all models are shown in Figure 2(b). In the material setting, bone model and drilling cutter material attributes were assigned according to the content in Table 1, respectively. Temperature displacement coupling was selected in the analysis step, and the cutting time was set to 0.02 s. In order to save calculation time, mass scaling of the model was required. The target time increment was set to 1E-006 in time increment mode. Temperature and force were selected from both the field and historical variables. Because this paper mainly studied the cutting temperature and cutting force in the process of bone drilling, and did not involve the tool wear, the drilling bit was set as rigid body. The tangential behavior between the drilling bit and the bone model was set as penalty function with the friction coefficient 0.3, and the normal behavior was set as hard contact. In the boundary condition setting, the six degrees of freedom of the bone model were completely fixed. The Z-axis direction of the drilling bit was set as the feed movement speed and the cutting speed rotating around the Z-axis, and the other degrees of freedom were fixed. The mesh type of drilling bit was tetrahedral element mesh C3D4T, and the number of mesh was 145,322. The mesh types of all bone models were hexahedral mesh unit C3D8R, wherein the mesh number of Voronoi bone model with gradient 0.7, 0.8 and 0.9 was 1,819,800, 1,842,800, 1,826,248, respectively, and the mesh number of solid bone model was 1,070,680.

3. Results and discussion

3.1. FEA and experimental verification of cancellous bone model designed by Voronoi method

To verify that the constructed Voronoi bone tissue model with gradient was more similar to the real cancellous bone model, pig hind leg bone was selected for bone drilling experiment in computer numerical control (CNC) machining center. The drilling bit specification used in the experiment was consistent with the finite element model. The cutting force was collected by Kistler 2825A-02 piezoelectric dynamometer, and the cutting temperature generated by bone drilling was monitored by infrared temperature sensor in real time. The cutting parameters of bone drilling experiment and FEA were set as cutting speed V_c = 20 r/s, feed speed V_f = 1.5 mm/s, and tip angle 2α = 115°. Table 5 shows the comparison of cutting temperature and cutting force between bone drilling experiment and FEA. The error calculation formula was as follows:

$$Error = \left| \frac{Result_{finite} - Result_{experiment}}{Result_{experiment}} \right| * 100\% \tag{5}$$

Where $Result_{finite}$ is the result of finite element analysis, including cutting temperature and cutting force; $Result_{experiment}$ is the result of cutting experiment, including cutting temperature and cutting force.

According to the data in Table 5, the cutting temperature and the cutting force generated by Voronoi bone models with different gradients in the FEA were both smaller than those of solid bone models, while the Voronoi bone models with gradient 0.8 was closer to the real bone structure by comparing with bone experiment. Because the interior of the real bone model was porous and dense, these voids reduced friction with the tool surface, which reduced friction heat and friction between bone and drilling bit. In the numerical analysis, there was no porous structure in the solid bone model, the contact area between the drilling bit surface and the solid bone model was large in the cutting process, which led to the large friction. Friction not only caused heat increase, but also resulted in greater friction force. The increase of heat directly led to the increase of cutting temperature, and the friction force, as a part of the source of cutting force, also triggered the increase of cutting force. In the finite element simulation of Voronoi bone models with different gradient, the bone tissue constructed by Voronoi method had porous structure inside, which was similar to the real bone tissue model. The results of FEA showed that the cutting temperature of Voronoi bone tissue was lower than that of solid model and closer to that of bone cutting experiment. Because these porous structures created by the Voronoi method were similar to the internal structure of real bone tissue, the interaction between the drilling bit surface and the bone model was reduced. In addition, by adjusting the gradient, the distribution of porous structures can be altered to mimic more real bone tissue. The FEA showed that the cutting temperature and cutting force of Voronoi bone model with gradient 0.8 was closer to the cutting experiments. The error values in Table 5 clearly verified this conclusion. Therefore, the cancellous bone model established by Voronoi method was of certain significance to the study of bone cutting. The subsequent cutting simulation of bone drilling was based on the Voronoi bone model with gradient 0.8. Because FEA technology has been widely used to simulate biomechanics, its results are reliable. In order to save the experiment time and cost, the cutting experiment comparison and verification of the finite element model is no longer carried out.

Table 5. Comparison of the cutting temperature and force.

	Cutting Temperature (°C)	Cutting Force (N)	Error (%)	
			Temp.	Force
Cutting experiment	47.7	34.5	--	--
Solid bone	57.1	47.4	19.70%	37.39%
Voronoi = 0.9 bone	53.8	38.9	12.79%	15.36%
Voronoi = 0.8 bone	51.6	31.3	8.17%	9.28%
Voronoi = 0.7 bone	43.2	29.8	9.43%	13.62%

3.2. The influence of cutting parameters on cutting temperature

According to the results in Section 3.1, under the same cutting conditions, the error between the cutting force and cutting temperature generated by Voronoi bone structure with gradient 0.8 and the results of bone drilling experiment was the smallest. Therefore, in the following orthogonal experiment of cutting parameters, the porous bone model with gradient 0.8 was taken as the research

object for FEA. According to the orthogonal cutting experiment scheme, Table 6 lists the cutting temperature results. In the range analysis table, K_i is the mean value of each factor at a certain level i, and R is range. The greater the range, the greater the influence of this factor on the test results. According to Table 7, the primary and secondary order of influence of each factor on cutting temperature was cutting speed > tip angle > feed speed. According to the FEA results of orthogonal experiment, the influence analysis of cutting parameters on cutting temperature was shown in Figure 3. As shown in Figure 3(a), when the tip angle was constant, the larger the cutting speed and feed speed were, the higher the cutting temperature would be in the process of bone drilling. As shown in Figure 3(b), when the feed speed was constant, the cutting temperature increased with the increase of the cutting speed. On the contrary, it tended to decrease with the increase of the tip angle. However, the combination of tip angle and feed speed had no stable effect on the cutting temperature of bone drilling.

By analyzing the influence of drilling parameters on cutting temperature, and combining with range method, the conclusion that cutting speed > tip angle > feed speed is obtained. The increase of cutting speed leads to the fracture of bone tissue caused by large shear deformation in a short time. As the cutting temperature of bone mainly comes from three regions, the shear deformation zone as shown in Figure 2(a), the deformation heat generated by the shear deformation of bone is the main source of heat. Larger shear deformation results in the rapid accumulation of cutting heat and the formation of higher cutting temperature. The tip angle mainly affects the contact area between the drilling bit and bone tissue and the heat dissipation area. The larger the tip angle is, the sharper the drilling bit is. At this time, the area of contact between the bit and bone tissue will be smaller, as shown in zone Ⅰ and zone Ⅱ in Figure 2(a). Therefore, tip angle affects the cutting temperature by changing the friction area between the bit and bone tissue. Feed speed, mainly by changing the speed of the cutting axial motion, has little influence on the shear deformation of bone tissue and the contact friction zone, so it has the least influence on the cutting temperature. Figure 4 also shows the finite element results of orthogonal experiments on Voronoi bone model drilling with gradient 0.8.

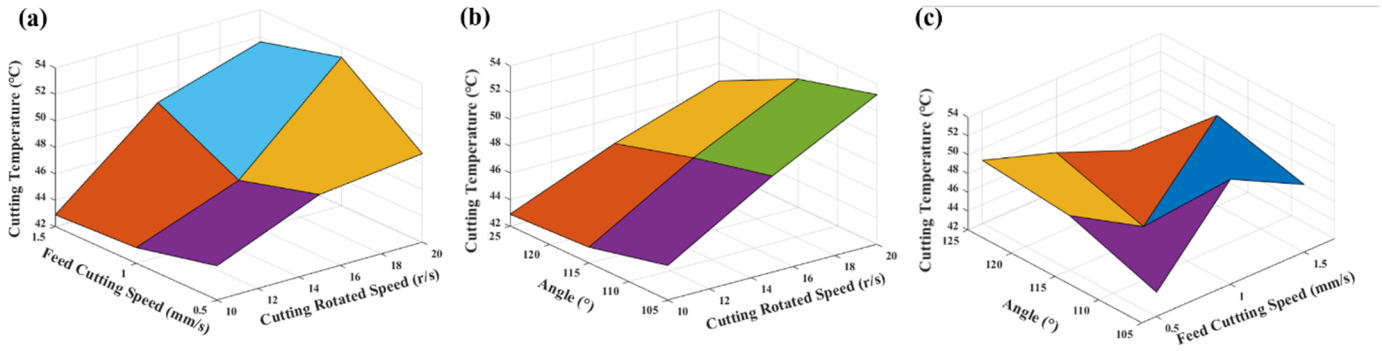

Figure 3. Analysis of influence of cutting parameters on cutting temperature: (a) cutting speed and feed speed-cutting temperature surface diagram; (b) cutting speed and tool tip angle-cutting temperature surface diagram; (c) feed speed and tip angle-cutting temperature surface diagram.

Table 6. Finite element simulation results of cutting temperature.

group	cutting speed V_c (r/s)	feed cutting V_f (mm/s)	tip angle 2α (°)	temperature (℃)
1	10	0.5	105	44.6
2	10	1.0	115	43.2
3	10	1.5	125	42.9
4	15	0.5	115	47.8
5	15	1.0	125	46.1
6	15	1.5	105	49.2
7	20	0.5	125	48.7
8	20	1.0	105	53.2
9	20	1.5	115	51.6

Table 7. Cutting temperature range analysis.

	K_i	cutting speed V_c (r/s)	feed speed V_f (mm/s)	tip angle 2α (°)
	K_1	130.7	141.1	147.0
tempeture	K_2	143.1	142.5	142.6
	K_3	153.5	143.7	137.7
	R	22.8	2.6	9.3
Weight of influence factor	W	$V_c > 2\alpha > V_f$		

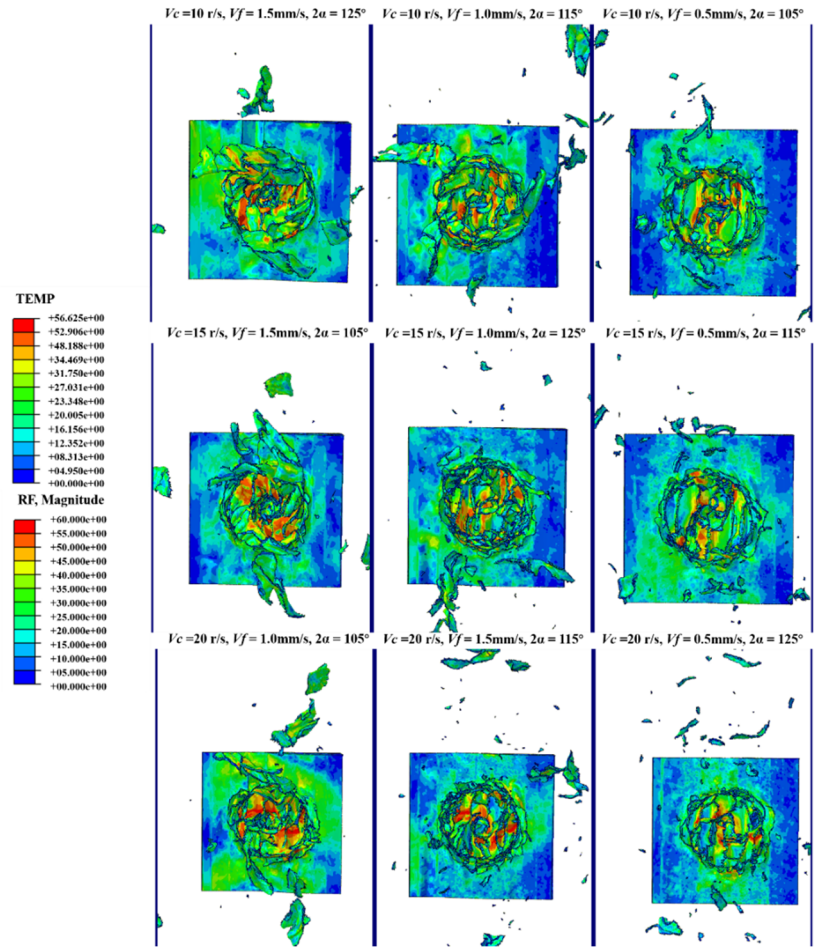

Figure 4. The cutting temperature and force of finite simulation.

3.3. The influence of cutting parameters on cutting forces

According to the orthogonal cutting experiment scheme, Table 8 lists the cutting force results. The proportion of influence of cutting parameters on cutting force is also analyzed by range method, as shown in Table 9. The order of influence of each factor on cutting force is tip angle > feed speed > cutting speed. According to the finite element simulation results of orthogonal experiment, the influence analysis of cutting parameters on cutting force is shown in Figure 5. When the speed is 15 r/s, the cutting force increases first and then decreases with the feed speed. Similarly, when the feed speed is 1 mm/s, the cutting force also increases first and then decreases with the increase of the cutting speed. Among other parameters, there is no obvious law of cutting force variation, as shown in Figure 5(a). From Figure 5(b),(c), it can be observed that when the tip angle is 125°, the cutting force is still greater than that when the tip angle is 115° and 105°, although the cutting speed and feed speed change. Specifically, when the tip angle is 125°, the cutting force increases with the increase of speed, but decreases with the increase of feed speed. By analyzing the influence of cutting parameters on cutting force, it can be found that the influence of multiple cutting parameters on cutting force should be considered simultaneously to obtain a relatively small cutting force.

Through the results of FEA, the influence of tip angle on cutting force is the largest. As tip angle changes affect the degree sharp of drilling bit. The larger the tip angle is, the sharper the

drilling bit is. Bone tissue under the action of sharp drilling bit occurs large deformation, resulting in the interaction force between the drilling bit and bone tissue becomes larger, that is, the cutting force becomes larger.

The feed speed mainly changes the cutting force by affecting the axial action of the drilling bit surface and bone tissue. Due to the porous structure inside the bone tissue, the distribution of porosity interacts with the bit surface in the axial direction, and the feed speed is too small, resulting in the bit interacting with more bone solid structures in the axial direction, which leads to a larger axial force. As the feed speed increases, the drilling bit tip passes through the pores, leaving more surface in the pores of bone tissue, which reduces the axial force generated when the drilling bit cuts bone tissue. The cutting speed mainly affects shear force of bone model. The tool rotates in the bone tissue, forming shear force to make bone tissue shear deformation. The drilling bit produces serious shear action on bone tissue at a faster cutting speed, thus forming a larger shear force, so that the cutting force becomes larger.

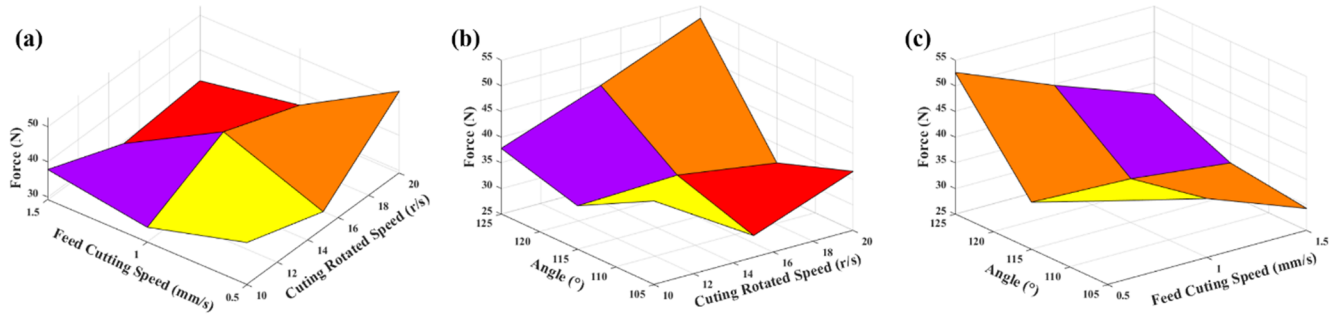

Figure 5. Analysis of influence of cutting parameters on cutting force: (a) cutting speed and feed speed-cutting force surface diagram; (b) cutting speed and tool tip angle-cutting force surface diagram; (c) feed speed and tip angle-cutting force surface diagram.

Table 8. Finite element simulation results of cutting force.

Group	Cutting speed V_c (r/s)	Feed cutting V_f (mm/s)	Tip angle 2α (°)	Force (N)
1	10	0.5	105	41.3
2	10	1.0	115	33.5
3	10	1.5	125	37.8
4	15	0.5	115	34.2
5	15	1.0	125	44.8
6	15	1.5	105	29.3
7	20	0.5	125	52.6
8	20	1.0	105	36.5
9	20	1.5	115	31.3

Table 9. Cutting force range analysis.

	K_i	Cutting speed V_c (r/s)	Feed speed V_f (mm/s)	Tip angle 2α (°)
	K_1	112.6	128.1	107.1
Force	K_2	108.3	114.8	99.0
	K_3	120.4	98.4	135.2
	R	12.1	29.7	36.2
Weight of influence factor	W	$2\alpha > V_f > V_c$		

4. Prediction model of cutting temperature and cutting force and optimization of cutting parameters

According to the experimental scheme of Table 4, the cutting temperature prediction model and the cutting force prediction model were established based on cutting parameters such as cutting speed, feed speed and tip angle, respectively. Since there is not a simple linear relationship between cutting temperature and cutting parameters, cutting force and cutting parameters, the prediction model of bone cutting temperature and cutting force were established:

$$T = V_c^a * V_f^b * (2\alpha)^c \tag{6}$$

Where T is the cutting temperature; a, b, and c are coefficients, respectively.

$$F = V_c^d * V_f^e * (2\alpha)^h \tag{7}$$

Where F is the cutting force; d, e, and h are coefficients, respectively.

Since Eqs (6) and (7) are non-highly nonlinear functions and complicated to calculate, they are converted into linear functions by means of the least square method. Here, the cutting temperature prediction model Eq (6) is taken as an example to calculate. Take the logarithm of Eq (6):

$$ln\, T = a\, ln\, V_c + b\, ln\, V_f + c\, ln\, 2 \tag{8}$$

Let $Y = ln\, T$, $x_1 = ln\, V_c$, $x_2 = ln\, V_f$, $x_3 = ln\, 2\alpha$, $b_1 = a$, $b_2 = b$, $b_3 = c$, so Equation (8) can be converted to Eq (9):

$$Y = b_1 x_1 + b_2 x_2 + b_3 x_3 \tag{9}$$

There are independent variables x_1, x_2 and x_3 in Eq (9). Since there are 9 experimental groups, the independent variables of group i are x_{i1}, x_{i2} and x_{i3}. Similarly, the cutting temperature Y obtained

by finite element calculation is expressed as Y_i. The specific expression is as follows:

$$y_i = b_i x_{i1} + b_i x_{i2} + b_i x_{i3} \qquad (i=1,2,3,4,5,6,7,8,9) \tag{10}$$

To simplify the calculation, Eq (10) is changed into a matrix, as follows:

$$Y = \begin{pmatrix} y_1 \\ \vdots \\ y_9 \end{pmatrix} \qquad B = \begin{pmatrix} b_1 \\ b_2 \\ b_3 \end{pmatrix}$$

$$X = \begin{bmatrix} x_{11} & x_{12} & x_{13} \\ \vdots & \ddots & \vdots \\ x_{91} & \cdots & x_{93} \end{bmatrix} \tag{11}$$

Finally, Eq (11) can be obtained:

$$B = (X^T X)^{-1} X^T Y \tag{12}$$

The data in Table 6 are substituted into Eq (12) to calculate the coefficient matrix b.

$$B = \begin{pmatrix} 0.2670 \\ 0.0135 \\ 0.6632 \end{pmatrix}$$

Therefore, the coefficient of the cutting temperature Eq (6) and the function relationship between the cutting temperature and the cutting parameters are finally obtained:

$$a = 1.3061,\ b = 1.0136,\ c = 1.9410$$

$$T = V_c^{1.3061} * V_f^{1.0136} * (2\alpha)^{1.9410}$$

Similarly, the function relation between cutting force and cutting parameters is obtained by the same method.

$$F = V_c^{1.0347} * V_f^{0.8010} * (2\alpha)^{2.0955}$$

In this section, based on the porous Voronoi bone models, the least square method was used to establish the prediction models of drilling parameters-cutting temperature and drilling parameters-cutting force, respectively.

5. Conclusions

Since bone drilling is a common surgical procedure, it is important to create a model that can mimic real bone tissue. Therefore, this study mainly established a bone model with gradient structure and dense porous interior based on Voronoi method. By using finite element analysis (FEA) technology, the cutting temperature and the cutting force generated by Voronoi bone model with gradient 0.8 were determined to be close to the real bone issue by simulating three bone models with

different gradients. Furthermore, the cutting parameters of bone drilling had a great influence on the cutting force and the cutting temperature. Orthogonal experiments were established to analyze the drilling parameters of Voronoi bone models in detail. Combined with range method, the proportion of influence of cutting parameters on cutting temperature and cutting force was obtained. Specifically, cutting speed had the greatest influence on cutting temperature, followed by tip angle. However, the tip angle has the greatest influence on the cutting force, followed by the feed speed. It can be seen that reasonable cutting parameters were very important to cutting temperature and cutting force. Finally, the least square method was used to predict the cutting temperature-cutting parameters, and cutting force-cutting parameters.

Although this study provides a theoretical analysis of bone drilling and validates the reliability of Voronoi bone structure, there are still some defects. In the future research, we will make use of biological 3D printing technology to create Voronoi bone models in vitro for mechanical experimental analysis and biological properties.

Acknowledgments

We would like to thank School of Mechanical and Vehicle Engineering of Changchun University for providing CNC machining center, dynamometer and other equipment. Thanks for the guidance of finite element simulation provided by colleagues.

Conflict of interest

The authors declare there is no conflict of interest.

References

1. J. E. Lee, Y. Rabin, O. B. Ozdoganlar, A new thermal model for bone drilling with applications to orthopaedic surgery, *Med. Eng. Phys.*, **33** (2011), 1234–1244. https://doi.org/10.1016/j.medengphy.2011.05.014
2. G. F. Tawy, P. J. Rowe, P. E. Riches, Thermal damage done to bone by burring and sawing with and without irrigation in knee arthroplasty, *J. Arthroplasty*, **31** (2016), 1102–1108. https://doi.org/10.1016/j.arth.2015.11.002
3. N. Bertollo, H. R. M. Milne, L. P. Ellis, P. C. Stephens, R. M. Gillies, W. R. Walsh, A comparison of the thermal properties of 2- and 3-fluted drills and the effects on bone cell viability and screw pull-out strength in an ovine model, *Clin. Biomech.*, **25** (2010), 613–617. https://doi.org/10.1016/j.clinbiomech.2010.02.007
4. M. Steeves, C. Stone, J. Mogaard, S. Byrne, How pilot-hole size affects bone-screw pullout strength in human cadaveric cancellous bone, *Can. J. Surg.*, **48** (2005), 207–212. Available from: https://www.ncbi.nlm.nih.gov/pmc/articles/PMC3211539/.
5. S. R. H. Davidson, D. F. James, Measurement of thermal conductivity of bovine cortical bone, *Med. Eng. Phys.*, **22** (2000), 741–747. https://doi.org/10.1016/S1350-4533(01)00003-0
6. A. Feldmann, P. Wili, G. Maquer, P. Zysset, The thermal conductivity of cortical and cancellous bone, *Eur. Cells Mater.*, **35** (2018), 25–33. https://doi.org/10.22203/eCM.v035a03

7. J. Soriano, A. Garay, P. Aristimuño, P. J. Arrazola, Study and improvement of surgical drill bit geometry for implant site preparation, *Int. J. Adv. Manuf. Technol.*, **74** (2014), 615–627. https://doi.org/10.1007/s00170-014-5998-x
8. M. F. A. Akhbar, A. R. Yusoff, Fast & Injurious: Reducing thermal osteonecrosis regions in the drilling of human bone with multi-objective optimization, *Measurement*, 152 (2020), 107385. https://doi.org/10.1016/j.measurement.2019.107385
9. J. Sui, N. Sugita, M. Mitsuishi, Thermal modeling of temperature rise for bone drilling with experimental validation, *J. Manuf. Eng.*, **137** (2015), 1–10. https://doi.org/10.1115/1.4030880
10. R. K. Pandey, S. S. Panda, Drilling of bone: a comprehensive review, *J. Clin. Orthop. Trauma*, **4** (2013), 15–30. https://doi.org/10.1016/j.jcot.2013.01.002
11. S. R. H. Davidson, D. F. James, Drilling in bone: modeling heat generation and temperature distribution, *J. Biomech. Eng.*, **125** (2003), 305–314. https://doi.org/10.1115/1.1535190
12. Y. C. Chen, Y. K. Tu, J. Y. Zhuang, Y. J. Tsai, C.Y. Yen, C. K. Hsiao, Evaluation of the parameters affecting bone temperature during drilling using a three-dimensional dynamic elastoplastic finite element model, *Med. Biol. Eng. Comput.*, **55** (2017), 1949–1957. https://doi.org/10.1007/s11517-017-1644-8
13. F. Karaca, B. Aksakal, M. Kom, Influence of orthopaedic drilling parameters on temperature and histopathology of bovine tibia: an in vitro study, *Med. Eng. Phys.*, **33** (2011), 1221–1227. https://doi.org/10.1016/j.medengphy.2011.05.013
14. T. Udiljak, D. Ciglar, S. Skoric, Investigation into bone drilling and thermal bone necrosis, *Investig. Bone Drill. Therm. Bone Necrosis*, **2** (2007), 103–112.
15. K. Alam, A. V. Mitrofanov, V. V. Silberschmidt, Finite element analysis of forces of plane cutting of cortical bone, *Comput. Mater. Sci.*, **46** (2009), 738–743. https://doi.org/10.1016/j.commatsci.2009.04.035
16. Y. Wang, M. Cao, X. Zhao, G. Zhu, C. McClean, Y. Zhao, et al., Experimental investigations and finite element simulation of cutting heat in vibrational and conventional drilling of cortical bone, *Med. Eng. Phys.*, **36** (2014), 1408–1415. https://doi.org/10.1016/j.medengphy.2014.04.007
17. Y. Wang, M. Cao, Y. Zhao, G. Zhou, W. Liu, D. Li, Experimental investigations on microcracks in vibrational and conventional drilling of cortical bone, *J. Nanomater.*, **2013** (2013), 845205. https://doi.org/10.1155/2013/845205
18. R. Zakrasas, V. Jurenas, J. Baskutiene, Analysis of compact bone vibration assisted drilli ng, *Solid State Phenom.*, **251** (2016), 183–187. https://doi.org/10.4028/www.scientific.net/SSP.251.183
19. V. Ostaševičius, G. Balevičius, R. Zakrasas, J. Baskutiene, V. Jurenas, Investigation of vibration assisted drilling prospects for improving machining characteristics of hard to machine materials at high and low frequency ranges, *Mechanika*, **22** (2016), 125–131. https://doi.org/10.5755/j01.mech.22.2.14431
20. V. Gupta, P. M. Pandey, Experimental investigation and statistical modeling of temperature rise in rotary ultrasonic bone drilling, *Med. Eng. Phys.*, **38** (2016), 1330–1338. https://doi.org/10.1016/j.medengphy.2016.08.012
21. H. Paktinat, S. Amini. Ultrasonic assistance in drilling: FEM analysis and experimental approaches. *Int. J. Adv. Manuf. Technol.*, **92** (2017), 2653–2665. https://doi.org/10.1007/s00170-017-0285-2

22. M. Nosouhi, R. Nosouhi, H. Paktinat, S. Amini, Finite element analysis and experimental investigation on the conventional and vibration assisted drilling, J. *Mod. Processes Manuf. Prod.*, **6** (2017), 22–33.
23. Z. Liao, D. A. Axinte, D. Gao, A novel cutting tool design to avoid surface damage in bone machining, *Int. J. Mach. Tools Manuf.*, **116** (2017), 52–59. https://doi.org/10.1016/j.ijmachtools.2017.01.003
24. Y. Hu, X. Chen, J. Chen, C. Zhang, W. Fu, The influence of crescent texture parameters on the axial force when drilling bone, *Med. Eng. Phys.*, **87** (**2021**), 87–94. https://doi.org/10.1016/j.medengphy.2020.12.001
25. N. Sugita, K. Ishii, J. Sui, M. Terashima, Multi-grooved cutting tool to reduce cutting force and temperature during bone machining, *CIRP Ann.*, **63** (2014), 101–104. https://doi.org/10.1016/j.cirp.2014.03.069
26. N. Sugita, T. Osa, R. Aoki, M. Mitsuishi, A new cutting method for bone based on its crack propagation characteristics, *CIRP Ann.*, **58** (2009), 113–118. https://doi.org/10.1016/j.cirp.2009.03.057
27. M. F. A. Akhbar, A. W. Sulong, Surgical drill bit design and thermomechanical damage in bone drilling: a review, *Ann. Biomed. Eng.*, **49** (2021), 29–56. https://doi.org/10.1007/s10439-020-02600-2
28. A. G. Robling, A. B. Castillo, C. H. Turner, Biomechanical and molecular regulation of bone remodeling, *Annu. Rev. Biomed. Eng.*, **8** (2006), 455–498. https://doi.org/10.1146/annurev.bioeng.8.061505.095721
29. X. Wang, S. Xu, S. Zhou, W. Xu, M. Leary, P. Choong, et al., Topological design and additive manufacturing of porous metals for bone scaffolds and orthopaedic implants: a review. *Biomaterials*, **83** (2016), 127–141. https://doi.org/10.1016/j.biomaterials.2016.01.012
30. S. Gómez, M. D. Vlad, J. López, E. Fernández, Design and properties of 3D scaffolds for bone tissue engineering, *Acta Biomater.*, **42** (2016), 341–350. https://doi.org/10.1016/j.actbio.2016.06.032
31. J. Y. Rho, L. Kuhn-Spearing, P. Zioupos, Mechanical properties and the hierarchical structure of bone, *Med. Eng. Phys.*, **20** (1998), 92–102. https://doi.org/10.1016/S1350-4533(98)00007-1
32. E. Bednarczyk, T. Lekszycki, A novel mathematical model for growth of capillaries and nutrient supply with application to prediction of osteophyte onset, *Z. Angew. Math. Phys.*, **67** (2016), 94–108. https://doi.org/10.1007/s00033-016-0687-2
33. I. Giorgio, M. Spagnuolo, U. Andreaus, D. Scerrato, A. M. Bersani, In-depth gaze at the astonishing mechanical behavior of bone: a review for designing bio-inspired hierarchical metamaterials, *Math. Mech. Solids*, **26** (2021), 1074–1103. https://doi.org/10.1177/1081286520978516
34. L. Placidi, F. Dell'Isola, N. Ianiro, G. Sciarra. Variational formulation of pre-stressed solid–fluid mixture theory, with an application to wave phenomena, *Eur. J. Mech. A. Solids*, **27** (2008), 582–606. https://doi.org/10.1016/j.euromechsol.2007.10.003
35. O. Devillers, M. Golin, K. Kedem, S. Schirra, Queries on Voronoi diagrams of moving points, *Comput. Geom.*, **6** (1996), 315–327. https://doi.org/10.1016/0925-7721(95)00053-4
36. F. Aurenhammer, Voronoi diagrams - a survey of a fundamental data structure, *ACM Comput. Surv.*, **23** (1991), 345–405. https://doi.org/10.1145/116873.116880

37. G. Wang, L. Shen, J. Zhao, H. Liang, D. Xie, Z. Tian, et al., Design and compressive behavior of controllable irregular porous scaffolds: based on Voronoi-tessellation and for additive manufacturing, *ACS Biomater. Sci. Eng.*, **4** (2018), 719–727. https://doi.org/10.1021/acsbiomaterials.7b00916
38. H. Zhao, Y. Han, C. Pan, D. Yang, H. Wang, T. Wang, et al., Design and mechanical properties verification of gradient Voronoi scaffold for bone tissue engineering, *Micromachines*, **12** (2021), 1–23. https://doi.org/10.3390/mi12060664
39. V. Prasannavenkadesan, P. Pandithevan, Johnson-cook model combined with cowper-symonds model for bone cutting simulation with experimental validation, *J. Mech. Med. Biol.*, **21** (2021), 1–23. https://doi.org/10.1142/S021951942150010X

AIMS Press